

Onset of convection in fluids with strongly temperature-dependent, power-law viscosity

2. Dependence on the initial perturbation

V.S. Solomatov^{a,*}, A.C. Barr^b

^a *Department of Earth and Planetary Sciences, Washington University in St. Louis, St. Louis, MO 63130, USA*

^b *Department of Space Studies, Southwest Research Institute, Boulder, CO 80302, USA*

Received 1 January 2007; received in revised form 4 May 2007; accepted 19 June 2007

Abstract

The onset of convection in the power-law creep regime on the silicate and icy planetary bodies requires a finite amplitude initial perturbation. This is a nonlinear problem and thus, both the amplitude and shape of the perturbation are important. We performed numerical simulations of the onset of convection in a two-dimensional layer with a fixed temperature contrast between the boundaries and in the stagnant lid regime of temperature-dependent viscosity convection. The optimal perturbations are located at the bottom of the layer (in the rheological sublayer) and have the wavelength of about twice the thickness of the rheological sublayer. The critical Rayleigh number for the onset of convection by optimal perturbations is calculated for a broad range of viscosity parameters. The results are summarized in terms of simple scaling relationships.

© 2007 Elsevier B.V. All rights reserved.

Keywords: Dislocation creep; Power-law viscosity; Onset of convection

1. Introduction

Constraints on the onset of convection in fluids with complicated rheologies are necessary to address long-standing questions about global convective stability of the interiors of terrestrial planets and icy satellites (Schubert et al., 1969; Reynolds and Cassen, 1979; McKinnon, 1999; Solomatov and Moresi, 2000; Barr et al., 2004; Barr and Pappalardo, 2005) as well as small-scale instabilities beneath continents and oceans on Earth (Jaupart and Parsons, 1985; Davaille and Jaupart, 1994; Lenardic and Moresi, 1999; Korenaga and Jordan, 2003; Huang et al., 2003; Sleep, 2005; Dumoulin et al., 2005)

and at the base of the mantle (Yuen and Peltier, 1980; Solomatov and Moresi, 2002).

Although the onset of convection in constant viscosity fluids (Chandrasekhar, 1961) and in temperature-dependent viscosity fluids (Stengel et al., 1982; Richter et al., 1983; White, 1988) has been well studied, the onset of convection in power-law viscosity fluids, where dislocation creep and/or grain boundary sliding accommodate strain, is not well understood. Dislocation creep is a strong competitor to diffusion creep in planetary mantles and it is not easy to draw the boundary between the two. The dislocation creep regime may dominate convective instabilities in silicate bodies if one takes into account grain growth, which tends to suppress diffusion creep but has no effect on dislocation creep (Karato and Wu, 1993). In the terrestrial planets, convective instabilities at the bottom

* Corresponding author.

E-mail address: slava@wustl.edu (V.S. Solomatov).

Nomenclature

a	aspect ratio of the convective box
a_{cr}	critical aspect ratio in linear stability analysis
a_{cr}^*	aspect ratio at the critical point
b	pre-factor in the viscosity function
c_p	isobaric specific heat
d	depth of the convective box
d_{sub}	thickness of the rheological sublayer
E	activation energy
F	heat flux
g	acceleration due to gravity
k	thermal conductivity
L	width of the convecting box
n	stress exponent
Nu	Nusselt number
Nu_{cr}^*	Nusselt number at the critical point
R	gas constant
Ra	Rayleigh number
Ra_{cr}	critical Rayleigh number
$Ra_{cr,n}$	absolute minimum critical Rayleigh number for stress-dependent viscosity
$Ra_{cr,0}$	a constant in the scaling law
Ra_{sub}	Rayleigh number for the sublayer
Ra_{δ}	perturbation-dependent critical Rayleigh number
Ra_{cr}^*	absolute minimum critical Rayleigh number
$Ra_{cr,th}^*$	theoretically estimated absolute minimum critical Rayleigh number
t	time
T	temperature
ΔT	temperature contrast between the upper and lower boundaries
T_{cond}	temperature of a conductive layer
ΔT_{sub}	temperature contrast across rheological sublayer
T_0	surface temperature
T_1	bottom temperature
T_{ξ}	temperature field with imposed perturbation
u	velocity
x	horizontal coordinate
y	vertical coordinate
y_l	lower boundary of the sinusoidal perturbation
y_u	upper boundary of the sinusoidal perturbation
α	thermal expansion
γ	coefficient in the viscosity function

δT	temperature perturbation
δT_{cr}	critical perturbation for the onset of convection
δT_{sin}	sinusoidal temperature perturbation
δT_{ξ}	temperature perturbation constructed from the critical solution
δT_{cr}^*	amplitude of temperature variation at the critical point
$\delta T'_{\xi}$	temperature perturbation with zero horizontal average
δT_0	amplitude of sinusoidal temperature perturbation
$\Delta \eta$	viscosity contrast between the upper and lower boundaries
η	viscosity
θ	Frank–Kamenetskii parameter
κ	coefficient of thermal diffusivity
λ	perturbation wavelength
λ_{cr}^*	optimal wavelength
ξ	coefficient controlling the amplitude of temperature perturbation
τ	second invariant of deviatoric stress tensor
τ_T	stress due to initial perturbation

of the lithosphere are controlled by dislocation creep if the grain size exceeds ~ 1 mm (Solomatov and Moresi, 2000). This is a possible situation because the grain size in the Earth's mantle varies from 0.1 mm to 1 cm (Karato and Wu, 1993). In icy satellites, convective instability may be governed by weakly non-Newtonian grain boundary sliding if ice grain sizes exceed 1 mm (Barr and Pappalardo, 2005; Barr and McKinnon, 2007).

The onset of convection in power-law viscosity fluids was investigated by Tien et al. (1969) and Ozoë and Churchill (1972). The onset of convection in the dislocation creep regime of Earth's materials was studied by Birger (1998, 2000). Birger's (1998, 2000) solutions describe the onset of convection for infinitesimal amplitudes, when the Andrade law is applicable (transient creep). However, even if the initial stage is described by the Andrade law, after about 10% strain the creep is in a steady-state regime (from the point of view of dislocation dynamics) and one has to investigate how the flow will evolve after that. Thus, one still needs to consider power-law viscosity.

Solomatov (1995) suggested an approximate equation for the onset of convection in the stagnant lid regime of temperature-dependent, power-law viscosity convection in a layer with a fixed temperature difference between the boundaries. In this regime, convection is

confined within a low viscosity sublayer at the bottom of the convective layer (the rheological sublayer), while the upper part of the layer is stagnant. According to the terminology which we use in this paper, Solomatov's (1995) equation gives the *absolute minimum critical Rayleigh number*, Ra_{cr}^* , below which all perturbations decay independently of the amplitude. This equation was tested numerically by Barr et al. (2004), Barr and Pappalardo (2005) and Solomatov and Barr (2006). In the latter work, we determined the absolute minimum critical Rayleigh number by starting with a steady-state convection solution and reducing the Rayleigh number in small steps until convection collapses. This approach does not require using any perturbation functions and gives the most accurate estimate of the absolute minimum critical Rayleigh number.

Although it is useful to know when convection does not occur, it might be more important to know when it does occur. This is a more difficult problem. Barr et al. (2004) and Barr and Pappalardo (2005) investigated the onset of convection by sinusoidal perturbations (for ice rheology). The use of sinusoidal functions is motivated by the standard linear theory where the stability is analyzed in terms of Fourier components (normal modes). However, the linear theory methods are not applicable to nonlinear problems where the interaction between normal modes become important. Both the amplitude and shape of the perturbations can play a large role and thus, there is an infinite choice of possible initial conditions that one can explore.

Given this complexity, we believe that it would be useful to focus on the most effective perturbations: if we can understand what type of perturbations are most effective at triggering convection, then we can have a better idea how to analyze other types of perturbations. Here we investigate how the shape of the perturbation affects the onset of convection and suggest preliminary constraints on the dependence of the critical Rayleigh number on the amplitude of the most effective perturbations for a broad range of viscosity parameters.

2. Model

We solve equations of thermal convection in the Boussinesq approximation in a rectangular box with free-slip boundaries and aspect ratio $a = L/d$ where d is the depth and L is the width of the box. The temperature of the upper boundary $T = T_0$ and the temperature of the lower boundary $T = T_1$. The viscosity is temperature and stress dependent:

$$\eta = b\tau^{1-n} \exp(-\gamma T), \quad (1)$$

where τ is the second invariant of the deviatoric stress tensor, n is the stress exponent, and γ controls the variation of viscosity due to temperature alone.

The exponential function (1) is an approximation to the original Arrhenius viscosity function. This approximation (Frank–Kamenetskii approximation) has been justified for various problems (Morris, 1982; Morris and Canright, 1984; Ansari and Morris, 1985; Fowler, 1985; Davaille and Jaupart, 1994; Reese et al., 1999). The parameter γ is related to the activation energy, E , in the laboratory-derived creep law:

$$\gamma = \frac{E}{RT_1^2}, \quad (2)$$

where R is the gas constant.

The equations of thermal convection are nondimensionalized using d for the length scale, d^2/κ for the time scale, where κ is the thermal diffusivity, and $\Delta T = T_1 - T_0$ for the temperature scale. The non-dimensional viscosity of the fluid is described by two parameters, the stress exponent, n , and the viscosity contrast due to temperature alone:

$$\Delta\eta = \exp(\theta), \quad (3)$$

where

$$\theta = \gamma\Delta T \quad (4)$$

is the Frank–Kamenetskii parameter. Typical values for rocks and ice are $\Delta\eta \approx 10^6 - 10^{16}$ (Solomatov and Moresi, 1997; Barr et al., 2004).

The Rayleigh number is defined as follows:

$$Ra = \frac{\alpha g \rho \Delta T d^{(n+2)/n}}{\kappa^{1/n} b^{1/n}}, \quad (5)$$

where α is the coefficient of thermal expansion, g is the acceleration due to gravity and ρ is the density.

The Nusselt number, which describes the nondimensional convective heat flux, is

$$Nu = \frac{Fd}{k\Delta T}, \quad (6)$$

where F is the heat flux, $k = \rho c_p \kappa$ is the thermal conductivity, and c_p is the isobaric specific heat. For vigorous convection, $Nu \gg 1$, for sluggish convection, $Nu \sim 1$ and in the absence of convection (a linear conductive temperature profile), $Nu = 1$.

The simulations are performed using the finite element code CITCOM (Moresi and Solomatov, 1995). We generally use $m = 64$ vertical elements and vary the number of elements in the horizontal direction (which has variable width a —the aspect ratio).

3. Bifurcation diagram for temperature-dependent, power-law viscosity fluids

Before we will discuss the perturbation-dependent onset of convection, it is useful to describe the behavior of our system (a two-dimensional convective box of aspect ratio a) in terms of nonlinear dynamics (e.g., (Drazin and Reid, 1981; Drazin, 1992; Strogatz, 1994)).

The *amplitude* of the motion of this system can be characterized by velocity amplitude which can be defined, for example, as an r.m.s. velocity. To characterize the state of the system, one can use other parameters such as the Nusselt number Nu (Eq. (6)). The behavior of the system is controlled by the Rayleigh number—the *control parameter*.

The behavior of the system can be analyzed using a *bifurcation diagram* in axes Rayleigh number (control parameter) and velocity (amplitude). One can also analyze the behavior of the system in axes Ra – Nu . Steady-state solutions of convection equations can be either stable or unstable to infinitesimal perturbations. A line formed by stable solutions on the bifurcation diagram is called a *stable branch*. The unstable solutions form an *unstable branch*. The stable steady-state solutions can easily be obtained in laboratory experiments or numerical simulations. The unstable steady-state convection solutions are formal solutions of the convection equations with $\partial T/\partial t = 0$. These solutions are unstable to infinitesimal perturbations and are impossible to obtain in laboratory experiments.

As an example, consider a bifurcation diagram for a two-dimensional constant viscosity box with free-slip boundaries (Fig. 1 (a)). The critical Rayleigh number and the critical aspect ratio are $Ra_{cr} = 657.5$ and $a_{cr} = \sqrt{2}$, respectively. The conductive solutions at $Ra < Ra_{cr}$ constitute a stable branch with $Nu = 1$. Convection begins at $Ra = Ra_{cr}$. At $Ra > Ra_{cr}$ the large-amplitude steady-state convective solutions are located on a stable branch originating at $Ra = Ra_{cr}$, $Nu = 1$. In the supercritical region, the conductive solutions are unstable to infinitesimal perturbations and form an unstable branch. Note that near $Ra = Ra_{cr}$ the Nusselt number corresponding to the stable branch increases linearly with Ra (Malkus and Veronis, 1958; Schlüter et al., 1965).

The point $Ra = Ra_{cr}$, $Nu = 1$ is called a bifurcation point. The stable branch corresponding to conductive solutions at $Ra < Ra_{cr}$ bifurcates into two branches—the unstable conductive branch and stable large-amplitude convective branch (note that the latter consists of two branches if one consider clockwise and counter-clockwise flows). This type of bifurcation is called a

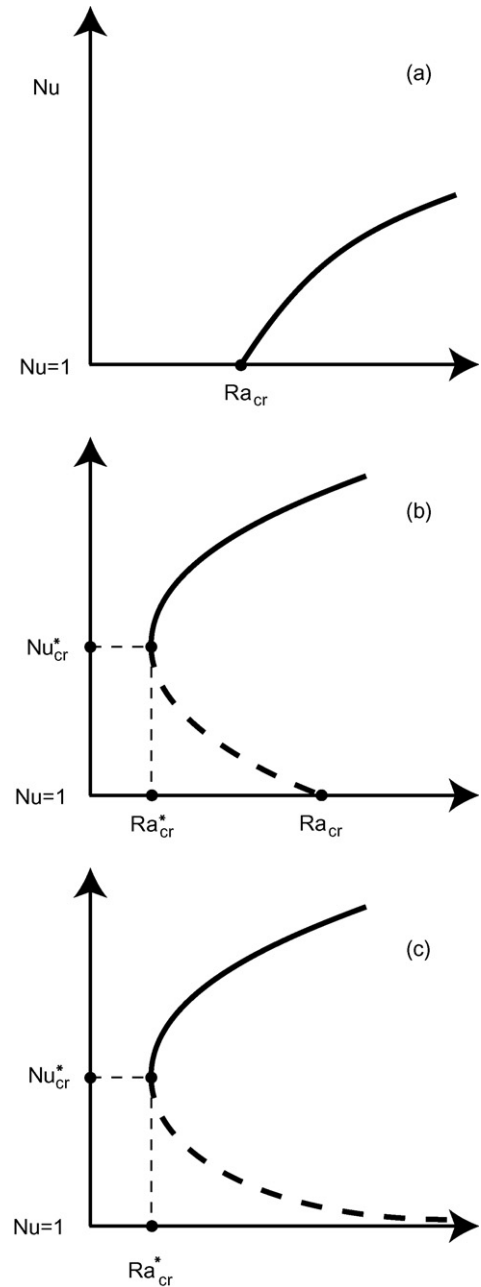


Fig. 1. Bifurcation diagram in Ra – Nu axes for (a) constant viscosity convection, (b) temperature-dependent viscosity convection and (c) power-law viscosity convection (with or without temperature dependence). The stable branches are shown with solid lines. Unstable branches are shown with dashed lines.

pitchfork bifurcation. Because the bifurcation extends in the supercritical region ($Ra > Ra_{cr}$), it is called *supercritical pitchfork bifurcation*.

For temperature-dependent viscosity fluids, there are two bifurcation points (Busse, 1967; Palm, 1975; Richter et al., 1983): $Ra = Ra_{cr}$, $Nu = 1$ and $Ra = Ra_{cr}^*$,

$Nu = Nu_{cr}^*$ (Fig. 1(b)). The point $Ra = Ra_{cr}$, $Nu = 1$ is a *subcritical pitchfork bifurcation*—it branches backward, in the subcritical region. Similarly to the constant viscosity case, the conductive solutions at $Ra > Ra_{cr}$ are unstable to infinitesimal perturbations. An important difference from the constant viscosity case is that in the range $Ra_{cr}^* < Ra < Ra_{cr}$ the conductive solutions are stable to infinitesimal perturbations but unstable to finite-amplitude perturbations. At $Ra < Ra_{cr}^*$, the conductive solutions are stable to both infinitesimal and finite-amplitude perturbations (this is called a globally asymptotically stable equilibrium). If the perturbations are sufficiently large, the system can reach a large-amplitude, steady-state convective solution. These solutions are located on the *stable subcritical branch*. In physical terms, the solutions in the subcritical region ($Ra_{cr}^* < Ra < Ra_{cr}$) are *metastable*. This phenomenon is common, for example, in phase transitions. In the subcritical region, both the conductive state (“phase α ”) and the convective state (“phase β ”) are stable to infinitesimal perturbations and thus, can be observed in laboratory experiments. However, a sufficiently large perturbation can trigger a transition from an initially conductive state to a convective state ($\alpha \rightarrow \beta$ transition) or from an initially convective state to a conductive state ($\beta \rightarrow \alpha$ transition).

The bifurcation point ($Ra = Ra_{cr}^*$, $Nu = Nu_{cr}^*$) is called a *saddle-node bifurcation*. It produces the stable subcritical branch and an unstable large-amplitude branch which connects the two bifurcation points (Fig. 1(b)). Note that with the increase of the Rayleigh number, the large-amplitude stable branch will bifurcate and produce branches which will too eventually bifurcate. The solutions will become periodic, quasiperiodic, and eventually, chaotic.

The bifurcation diagram for power-law viscosity (with or without temperature-dependence, Fig. 1(c)) differs from Newtonian temperature-dependent viscosity in that $Ra_{cr} = \infty$ (Lyubimova, 1974; Birger, 1993) and thus, all finite-amplitude solutions are essentially subcritical.

The bifurcation point ($Ra = Ra_{cr}^*$, $Nu = Nu_{cr}^*$) will be called here simply the *critical point*. The large-amplitude convection solution corresponding to this point will be called the *critical solution*.

4. The critical point

To obtain criteria for the onset of convection by finite-amplitude perturbations, we start with the critical point, $Ra = Ra_{cr}^*$. A theoretical expression for the absolute minimum critical Rayleigh number, Ra_{cr}^* , was suggested

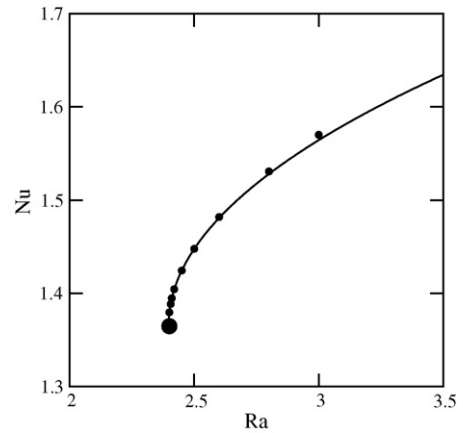


Fig. 2. Numerically determined Nusselt number as a function of the Rayleigh number in the vicinity of the critical point for $n = 3$, $\exp(\theta) = 10^{10}$ and $a = 0.61$ (small solid circles). The parabolic fit (based on the lowest four points, solid line) gives an accurate location of the critical point (large solid circle).

by Solomatov (1995):

$$Ra_{cr,th}^* = Ra_{cr,n} \left[\frac{e\theta}{4(n+1)} \right]^{2(n+1)/n} \exp\left(-\frac{\theta}{n}\right), \quad (7)$$

where $Ra_{cr,n} = Ra_{cr,1}^{1/n} Ra_{cr,\infty}^{(n-1)/n}$, $Ra_{cr,1} = 1568$, and $Ra_{cr,\infty} = 20$.

Solomatov and Barr (2006) determined Ra_{cr}^* numerically by starting with a steady-state convection solution and reducing the Rayleigh number in small steps until they reach the critical Rayleigh number at which convection collapses. Finding the aspect ratio at which the critical Rayleigh number is minimum gives both Ra_{cr}^* and the corresponding aspect ratio a_{cr}^* (Solomatov and Barr, 2006).

Solomatov and Barr’s (2006) results are accurate only to two significant digits. To improve the accuracy of Ra_{cr}^* , we performed additional calculations and estimated Ra_{cr}^* using parabolic functions in the vicinity of the critical point (Fig. 2). The values of the absolute minimum critical Rayleigh number, Ra_{cr}^* , calculated to three significant digits for $n = 2-4$ and $\exp(\theta) = 10^{10} - 10^{40}$ (including errors due to numerical resolution) are given in Table 1. The results can be summarized in terms of a correction factor for Eq. (7) (Fig. 3):

$$Ra_{cr}^* = (n+1)\theta^{-0.3} Ra_{cr,th}^*. \quad (8)$$

Note that the slope systematically decreases with θ for all n , so the coefficient 0.3 in Eq. (8) is an average value in the range between $\exp(\theta) = 10^{10}$ and 10^{40} . The case $n = 1$ is noticeably different from $n > 1$ and is not accurately described by the above formula. This might be related to fundamental differences between $n = 1$ and $n > 1$:

Table 1
Numerical results

n	$\log(\Delta\eta)$	Ra_{cr}^*	a_{cr}^*	Nu_{cr}^*	ΔT_{cr}^*
1	10	2.94×10^{-4}	0.41	1.19	0.158
1	12	5.61×10^{-6}	0.35	1.17	0.130
1	14	9.77×10^{-8}	0.31	1.16	0.112
1	16	1.58×10^{-9}	0.28	1.14	0.097
1	18	2.43×10^{-11}	0.26	1.13	0.088
1	20	3.57×10^{-13}	0.24	1.12	0.079
2	10	2.90×10^{-1}	0.53	1.29	0.189
2	20	1.81×10^{-5}	0.31	1.16	0.098
2	30	5.50×10^{-10}	0.22	1.12	0.065
2	40	1.23×10^{-14}	0.17	1.09	0.048
3	10	2.40	0.61	1.37	0.238
3	20	5.49×10^{-3}	0.36	1.21	0.114
3	30	6.80×10^{-6}	0.26	1.14	0.076
3	40	6.42×10^{-9}	0.20	1.11	0.056
4	10	6.25	0.68	1.43	0.263
4	20	8.62×10^{-2}	0.41	1.24	0.129
4	30	6.77×10^{-4}	0.30	1.17	0.089
4	40	4.15×10^{-6}	0.24	1.13	0.063

for $n = 1$, the subcritical region exists only because of the dependence of the viscosity on temperature while for $n > 1$, the subcritical region exists even when the viscosity does not depend on temperature (Appendix A).

The amplitude of the temperature variation at the critical point is defined as the maximum amplitude of horizontal temperature variation:

$$\delta T_{cr}^* = \max |T_{cr}^*(0, z) - T_{cr}^*(a, z)|. \quad (9)$$

Fig. 4 shows that δT_{cr}^* scales very well with the vertical temperature contrast across the rheological sublayer, Eq. (21):

$$\delta T_{cr}^* = 0.9(n + 3)\theta^{-1}. \quad (10)$$

Although the fact that δT_{cr}^* scales with θ^{-1} is not surprising, the fact that it varies with n as $(n + 3)$ rather than, say, $(n + 1)$ (Solomatov, 1995; Solomatov and Moresi, 2000) and that the coefficient $(n + 3)$ fits both $n = 1$ and $n > 1$ cases quite well is not obvious from our simple derivations. These coefficients need to be constrained better by more sophisticated theories.

Using Eqs. (2) and (4), Eq. (10) can be written in dimensional form as follows:

$$\delta T_{cr}^* = 0.9(n + 3) \frac{RT_1^2}{E}. \quad (11)$$

5. Perturbation function

For infinite Prandtl number fluids (or, more accurately, low Reynolds number flows), one can only issue a temperature perturbation but not a velocity perturbation.

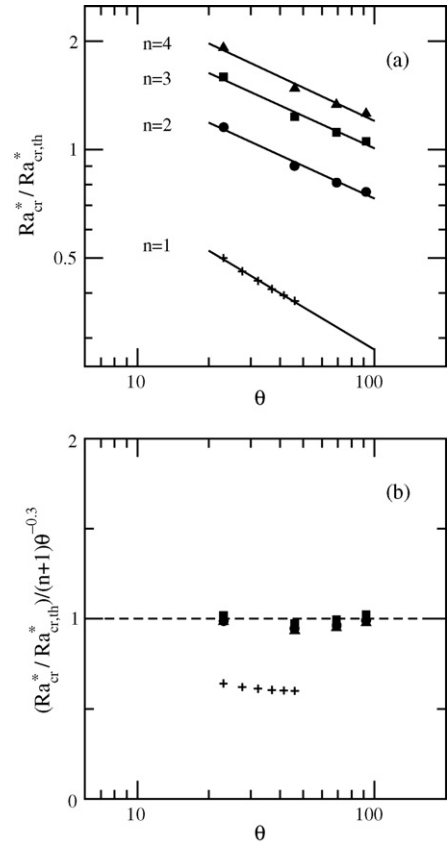


Fig. 3. (a) Ratio of the calculated absolute minimum critical Rayleigh number, Ra_{cr}^* , to the theoretical value, $Ra_{cr,th}^*$, for $n = 1$ (pluses), 2 (circles), 3 (squares) and 4 (triangles). The solid lines are the fitting curves: $Ra_{cr}^*/Ra_{cr,th}^* = a\theta^{-b}$ with $(a, b) = (1.7, 0.39)$, $(2.9, 0.30)$, $(4.0, 0.30)$, $(5.0, 0.31)$ for $n = 1, 2, 3$ and 4 , respectively. (b) The ratio $Ra_{cr}^*/Ra_{cr,th}^*$ normalized by $(n + 1)\theta^{-0.3}$.

This is due to the fact that the system does not have any inertia (the acceleration term is absent in mantle dynamics equations). The velocity field is established due to the balance between driving and resisting forces and thus, is uniquely determined by the temperature field.

Even though we only need to specify a temperature perturbation, the onset of convection by finite-amplitude temperature perturbations is a complex nonlinear problem. The approach that we believe is the most useful here is to try to identify the *optimal perturbations* which are the smallest disturbances of an initially conductive temperature distribution that would trigger convection for a given Rayleigh number.

To get some physical insight into how the optimal perturbations might look, we will take advantage of the basic structure of convection at large viscosity contrasts, i.e., in the stagnant lid regime of temperature-dependent viscosity convection. In this regime, convection is confined

to the rheological sublayer at the bottom. This suggests that the perturbations located outside of the rheological sublayer, i.e., in the stagnant lid, cannot be very effective at driving the convective motion. Unless the perturbation amplitude is so large (perhaps, on the order of the temperature contrast across the layer) that it would mobilize the lid, a perturbation localized within the lid is a “waste”—it is applied to a region which has a very high viscosity and thus, cannot convect. To be effective, the perturbation has to be located in the rheological sublayer.

An additional insight into this problem comes from the bifurcation diagram (Fig. 1). For a simple one-dimensional dynamic system whose motion is described by only one parameter, the steady-state solutions located on the unstable branch are, in fact, the perturbations which need to be issued to the system to destabilize it and move it to the large-amplitude stable branch. Although our system is more complicated, the most effective per-

turbations should, to some extent, resemble the actual steady-state convective solutions located on the unstable branch of the bifurcation diagram (Fig. 1(c)).

Although we cannot calculate the unstable steady-state solutions using fully time-dependent convection equations, the temperature field of the near-critical steady-state solution that we reached on the stable subcritical branch is a reasonable approximation for the temperature field of the unstable steady-state solutions, at least near the critical point. The structure of the convective solution at $Ra \approx Ra_{cr}^*$ is characterized by roughly equidimensional convective cells located inside the rheological sublayer. We assume that this structure is preserved along the subcritical branch at $Ra > Ra_{cr}^*$ and that the thickness of the rheological sublayer remains roughly constant. This is certainly the case for $n = 1$ where the solutions on both ends of the unstable subcritical branch are known exactly (Solomatov and Barr, 2006) and is likely to be the case for $n > 1$ as well. This can, in principle, be tested by solving convection equations with $\partial T/\partial t$ artificially set to zero.

Using these ideas, an optimal perturbation can be constructed as follows. In the absence of any convective motion the temperature field is described by a conductive temperature profile:

$$T_{\text{cond}} = y. \tag{12}$$

In the presence of convection the temperature $T(x, y)$ of the system deviates from the conductive profile by $\delta T(x, y)$:

$$T(x, y) = T_{\text{cond}} + \delta T(x, y). \tag{13}$$

To construct the optimal perturbation, we use the deviation of the temperature field $T_{cr}^*(x, y)$ of the steady-state solution near the critical point, $Ra = Ra_{cr}^*$, from T_{cond} and reduce its amplitude by some small coefficient $\xi < 1$:

$$\delta T_{\xi}(x, y) = \xi [T_{cr}^*(x, y) - T_{\text{cond}}]. \tag{14}$$

The total temperature field corresponding to this perturbation is

$$T_{\xi}(x, y) = T_{\text{cond}} + \delta T_{\xi}(x, y). \tag{15}$$

When $\xi = 0$, the initial temperature field is purely conductive. When $\xi = 1$, the initial temperature field is identical to the solution at the critical point ($Ra = Ra_{cr}^*$, $a = a_{cr}^*$). For a given perturbation amplitude, $\xi < 1$, one can find the critical Rayleigh number, Ra_{δ} at which the system becomes unstable. An example of such calculations is shown in Fig. 5.

Although the perturbations based on the critical solution are very efficient, it is interesting to explore other perturbations as well. Below we conduct a simple test

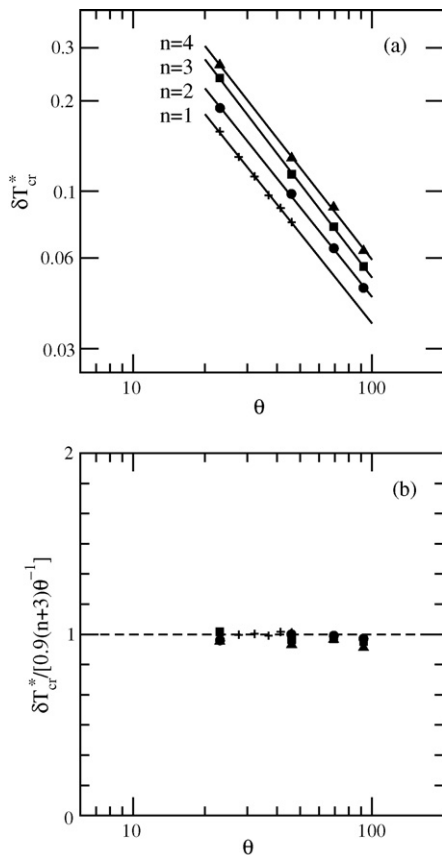


Fig. 4. (a) Dependence of the amplitude of the horizontal temperature variation, δT_{cr}^* , at the critical point on θ for $n = 1$ (pluses), 2 (circles), 3 (squares) and 4 (triangles). The slope of the fitting curves is -1 within 1–2% for all n . (b) The amplitude of the horizontal temperature difference, δT_{cr}^* , normalized by $0.9(n + 3)\theta^{-1}$.

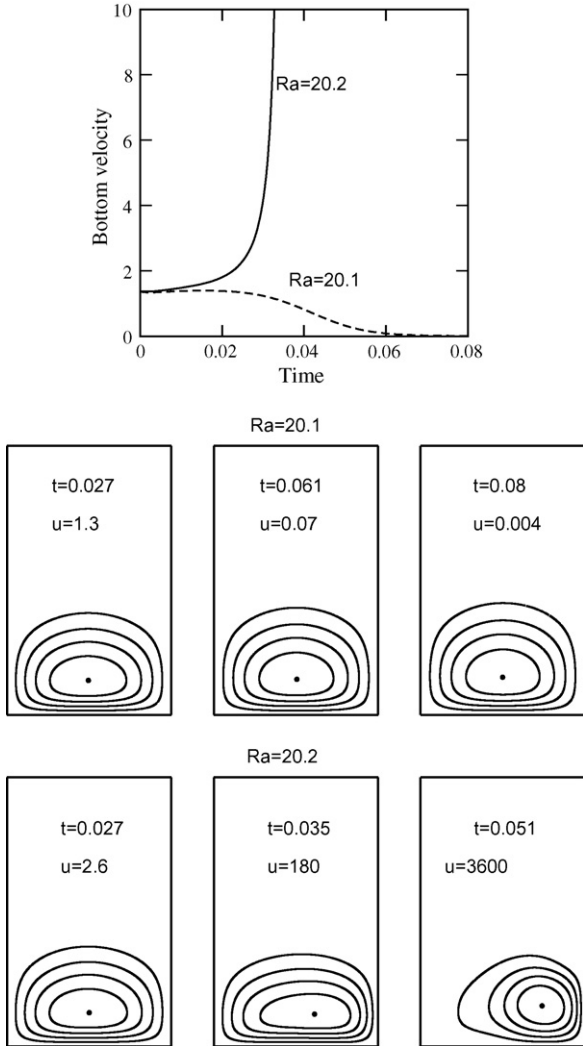


Fig. 5. The top graph shows the r.m.s. bottom velocity as a function of time for $n = 3$, $\exp(\theta) = 10^{10}$, $a = 0.61$ and $Ra = 20.1$ (decaying perturbation, solid line) and 20.2 (growing perturbation, dashed line). The initial perturbation is constructed using the temperature field at the critical point and reducing its magnitude by a factor of $\xi = 0.08$. The snapshots of the stream function at different times are shown for $Ra = 20.1$ (middle set) and 20.2 (bottom set). The time and the r.m.s. bottom velocity are indicated on each figure.

in which we compare the critical Rayleigh numbers for different initial perturbations for the case $n = 3$, $\exp(\theta) = 10^{20}$ and $a = 0.36$.

The first type of temperature perturbation is constructed as described above—by taking the near-critical stable solution and reducing the temperature anomaly of the near-critical convective solution by a factor of $\xi = 0.1$ (Eq. (14)). The temperature field of this perturbation is shown in Fig. 6 (a).

The perturbation (14) is characterized by both horizontal and vertical temperature variations (Fig. 6(a)). In most gravity-driven instabilities, the horizontal density variations are the ones which are most important. Therefore, we can try a perturbation similar to Eq. (14) but with a zero horizontal average ($\int_0^a \delta T(x, y) dx = 0$):

$$\delta T'_\xi(x, y) = \delta T_\xi(x, y) - \int_0^a \delta T_\xi(x, y) dx. \quad (16)$$

A perturbation constructed in this manner is shown in Fig. 6(b).

A different set of perturbations can be constructed using a sinusoidal function:

$$\delta T_{\sin}(x, y) = \delta T_0 \sin\left(\frac{\pi x}{a}\right) \sin\left[\frac{\pi(y - y_l)}{(y_u - y_l)}\right], \quad (17)$$

which is confined within a sublayer $y_l < y < y_u$. The perturbation is zero outside of this sublayer. The amplitude δT_0 is adjusted so that it matches the amplitude of the perturbations (14) and (16).

In one case, a sinusoidal perturbation, Eq. (17), is issued to the rheological sublayer (Fig. 6(c)). The shape of this perturbation is somewhat similar to the shape of the perturbation based on the critical solution with zero horizontally average temperature (Fig. 6(b)). In the other case, the sinusoidal perturbation is the same as in the previous case except that it is shifted to the middle of the layer (the lower portion of the stagnant lid, Fig. 6(d)).

Calculations using these four initial temperature perturbations (Fig. 6) show that the shape of the perturbation is not very important provided the perturbation is located within the rheological sublayer: the values of the critical Rayleigh number for the first three cases (Fig. 6(a)–(c)) are similar within 20%. The perturbations in Fig. 6(b) and (c) are substantially smaller (e.g., in terms of the total energy associated with a perturbation) and thus, are more optimal than the perturbation in (Fig. 6(a)).

The perturbation located in the stagnant part of the layer (Fig. 6(d)) is very ineffective in driving fluid motion. This suggests that starting convection from temperature fluctuations located in the stagnant lid may require Rayleigh numbers orders of magnitude larger than a similar-amplitude perturbation located in the rheological sublayer. Also, the onset of convection is substantially delayed in this case. The onset of convection by an arbitrary perturbation will depend on whether or not the initial perturbation will eventually reach a sufficiently large amplitude in the rheological sublayer.

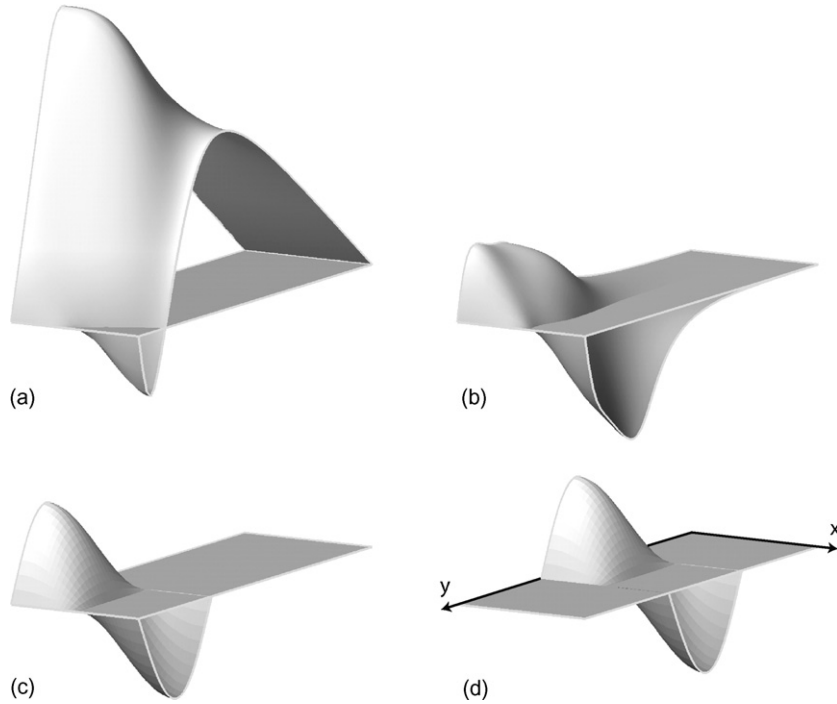


Fig. 6. Four finite amplitude temperature perturbations $\delta T(x, y)$ used to initiate convection for $n = 3$, $\exp(\theta) = 10^{20}$ and $a = 0.36$. The temperature scale (vertical axis) is the same for all plots. (a) The perturbation is constructed using the temperature variation of a near-critical solution for $Ra = 5.5 \times 10^{-3}$ and reducing its amplitude by a factor of $\xi = 0.1$, (b) Same as (a) but the horizontally averaged temperature is removed from the perturbation so that $\int_0^a \delta T(x, y) dx = 0$. (c) A simple sinusoidal perturbation is introduced at the bottom of the layer (the rheological sublayer), whose peak-to-peak amplitude is approximately the same as for (b). (d) The sinusoidal perturbation is shifted to the middle of the layer. The values of the critical Rayleigh number for the onset of convection are similar in the first three cases (0.054, 0.062 and 0.064, respectively), but in the last case it is one order of magnitude larger (~ 0.61).

6. Critical Rayleigh number for the onset of convection

Numerical simulations show that when the perturbation of amplitude δT is issued to the rheological sublayer, the perturbation grows or decays almost immediately. This means that the apparent viscosity of the rheological sublayer can be calculated using the characteristic stress associated with the initial perturbation:

$$\tau_T \sim \alpha \rho g \delta T d_{\text{sub}}, \quad (18)$$

where d_{sub} is the thickness of the rheological sublayer.

Following Stengel et al. (1982) and Solomatov (1995), we determine the Rayleigh number of the rheological sublayer at the mean temperature, $T = 1 - d_{\text{sub}}/2d$, of the sublayer and at the characteristic stress $\tau = \tau_T$, Eq. (18):

$$Ra_{\text{sub}} = \left\{ \frac{\alpha \rho g (dT/dy) d_{\text{sub}}^4}{\kappa b \tau_T^{1-n} \exp[-\theta(1 - d_{\text{sub}}/2d)]} \right\}^{1/n}, \quad (19)$$

where $dT/dy = \Delta T/d$ is the temperature gradient in the layer. Although it is not important here, we used the power $1/n$ to ensure that this Rayleigh number is reduced to the usual Rayleigh number for power-law viscosity (e.g., Solomatov, 1995) when $\tau_T = \alpha \rho g (dT/dy) d_{\text{sub}}^2$.

The rheological sublayer is the most unstable part of the layer. Its thickness is determined from the requirement that $\partial Ra_{\text{sub}}/\partial d_{\text{sub}} = 0$:

$$d_{\text{sub}} = 2(n+3)\theta^{-1}d. \quad (20)$$

The temperature difference ΔT_{sub} across the rheological sublayer is

$$\Delta T_{\text{sub}} = 2(n+3)\theta^{-1}\Delta T. \quad (21)$$

Eq. (20) gives us the thickness of the sublayer with the largest Rayleigh number (the most unstable sublayer). Substituting the value of (20) back into Eq. (19) gives us the Rayleigh number for the sublayer. The onset of convection can be determined by requiring that this sublayer is at the boundary of convective stability:

$$Ra_{\text{sub}} = Ra_{\text{cr},0}, \quad (22)$$

where $Ra_{cr,0}$ is a constant (presumably of the order of the critical Rayleigh number $Ra_{cr,n}$ which appears in Eq. (7)).

We obtain that the critical Rayleigh number for the entire layer is

$$Ra_{\delta} = Ra_{cr,0} \left[\frac{e\theta}{2(n+3)} \right]^{(n+3)/n} e^{-\theta/n} \left[\frac{\Delta T}{\delta T} \right]^{(n-1)/n}. \quad (23)$$

To simplify this equation, we can normalize it using $Ra = Ra_{cr}^*$, Eq. (7), and $\delta T = \delta T_{cr}^*$, Eq. (10), at the critical point:

$$\frac{Ra_{\delta}}{Ra_{cr}^*} \propto \left(\frac{\delta T_{cr}^*}{\delta T} \right)^{(n-1)/n}. \quad (24)$$

In this equation, we omitted the poorly constrained dependence of the pre-factor on n and did not include the correction factor, Eq. (8) (which would probably affect both Eqs. (23) and (8)).

The coefficient in Eq. (24) is constrained numerically. For fixed values of n and θ we ran a series of calculations to determine the critical Rayleigh number Ra_{δ} for the onset of convection as a function of ξ , using perturbation function (15), which is constructed using the temperature field of the near-critical solution at $Ra = Ra_{cr}^*$ (the last stable solution before convection collapses). Alternatively, one could use the perturbation function (14) or (16). However, as we discussed earlier, the difference among all these perturbations is small (Fig. 6).

The results are summarized in Fig. 7. For small amplitudes ($\delta T \ll \delta T_{cr}^*$), Eq. (24) compresses the numerical data reasonably well (Fig. 7):

$$\frac{Ra_{\delta}}{Ra_{cr}^*} \approx 3 \left(\frac{\delta T_{cr}^*}{\delta T} \right)^{(n-1)/n}, \quad (25)$$

where the pre-factor 3 fits the curves with the lowest values of $\exp(\theta) = 10^{10}$ and 10^{20} (which are more typical for planetary materials) and 2.5 is the mean value (2.5 ± 1 includes all curves).

Note that Eq. (24) is applicable for small-amplitude perturbations and is not accurate near the critical point (Fig. 7). For $n = 1$, the onset of convection depends on the initial perturbations only in a very narrow range, $Ra_{cr}^* < Ra < Ra_{cr}$ (essentially, $Ra_{cr}^* \sim Ra_{cr}$) and is not described by the above formula.

7. Dependence of the critical Rayleigh number on the perturbation wavelength

The wavelength $\lambda = 2a$, of the optimal perturbations is about twice the thickness of the rheological sublayer

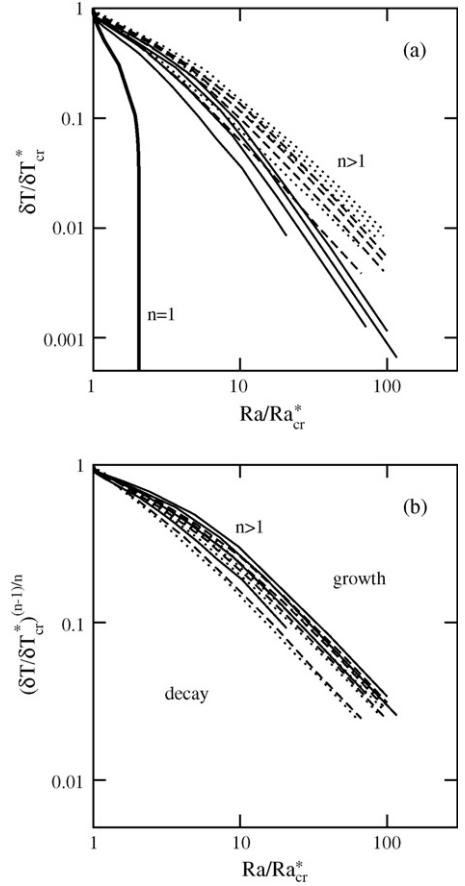


Fig. 7. (a) Summary of numerical constraints on the boundary separating decaying and growing initial perturbations: $n = 2$ (solid line), 3 (dashed line) and 4 (dotted line). For each n , calculations were performed for $\exp(\theta) = 10^{10}$, 10^{20} , 10^{30} and 10^{40} (the boundaries migrate upward with θ). The Rayleigh number is normalized by the absolute minimum critical Rayleigh number Ra_{cr}^* . The temperature perturbation is normalized by the temperature perturbation corresponding to the critical solution at $Ra = Ra_{cr}^*$ so that $\delta T / \delta T_{cr}^* = \xi$. A case with $n = 1$ and $\exp(\theta) = 10^{10}$ is shown for comparison (thick solid line). In the latter case, at $Ra > Ra_{cr} \approx 2Ra_{cr}^*$, convection can be initiated by infinitesimal perturbations. (b) The data for $n = 2, 3$ and 4 are shown in axes Ra / Ra_{cr}^* and $(\delta T / \delta T_{cr}^*)^{(n-1)/n}$.

which is only 15 km or so (Solomatov and Moresi, 2000). The wavelength of the initial perturbations can be quite large reaching, perhaps, the size of the planet. Thus, it would be interesting to estimate how the onset of convection depends on the perturbation wavelength. While we cannot reach the wavelengths of the size of the planet and we do not have a theory which would describe the dependence of the critical Rayleigh number on the wavelength it is still possible to get some constraints on how the critical Rayleigh number varies with the wavelength.

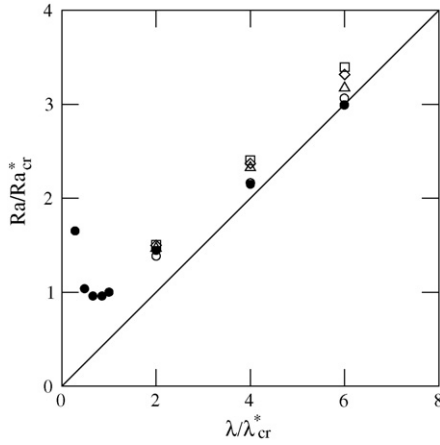


Fig. 8. Dependence of the critical Rayleigh number for the onset of convection on the wavelength of the sinusoidal perturbation located in the rheological sublayer for 5 cases: $n = 2$, $\exp(\theta) = 10^{10}$ (●), $n = 2$, $\exp(\theta) = 10^{20}$ (○), $n = 3$, $\exp(\theta) = 10^{10}$ (△), $n = 3$, $\exp(\theta) = 10^{20}$ (□), and $n = 4$, $\exp(\theta) = 10^{20}$ (◇). The Rayleigh number and the wavelength are normalized by their values at the critical point, Ra_{cr}^* and $\lambda_{cr}^* = 2a_{cr}^*$, respectively. The solid line is a linear function $Ra/Ra_{cr}^* = 0.5\lambda/\lambda_{cr}^*$. In one case, $n = 2$, $\exp(\theta) = 10^{10}$, the calculations extend to small values of λ/λ_{cr}^* and show that the minimum of Ra/Ra_{cr}^* is located close to $\lambda/\lambda_{cr}^* = 1$ and $Ra/Ra_{cr}^* = 1$. In all cases, the amplitude of the sinusoidal perturbation is 0.1 times the amplitude of the critical solution.

The simplest way to construct large wavelength perturbations is to use sinusoidal perturbations (Eq. (17) and Fig. 6(c)), confined to the rheological sublayer. Results for aspect ratios up to $a = 6a_{cr}^*$ ($\lambda = 12a_{cr}^* \sim 200$ km) are shown in Fig. 8. They suggest that for small amplitudes and large wavelengths:

$$\frac{Ra_{\delta}}{Ra_{cr}^*} \approx 1.5 \left(\frac{\lambda}{\lambda_{cr}^*} \right) \left(\frac{\delta T_{cr}^*}{\delta T} \right)^{(n-1)/n}, \quad \lambda > \lambda_{cr}^*, \quad (26)$$

where

$$\lambda_{cr}^* = 2a_{cr}^* \quad (27)$$

is the optimal wavelength.

This relationship is accurate within a factor of 2 and cannot be applied to very large λ/λ_{cr}^* because the dependence of Ra_{δ}/Ra_{cr}^* on λ/λ_{cr}^* is likely to be nonlinear.

We also estimated the minimum of the function $Ra_{\delta}(\lambda)$ for one case (Fig. 8). As expected, the minimum is reached near $\lambda/\lambda_{cr}^* \sim 1$.

The scaling laws (25) and (26) can be inverted so that one can estimate how large a perturbation needs to be issued to a layer with a particular Rayleigh number, Ra , to initiate convection. From Eq. (26) we find that the

critical (dimensional) temperature perturbation is

$$\delta T_{cr} \approx 10 \frac{RT_1^2}{E} \left(\frac{Ra_{cr}^* \lambda}{Ra \lambda_{cr}^*} \right)^{n/(n-1)}. \quad (28)$$

8. Discussion and conclusion

Unlike constant viscosity fluids where there is a single critical Rayleigh number for the onset of convection, whether convection occurs in fluids with variable viscosity can depend on the perturbation amplitude. In power-law viscosity fluids, initiation of convection is always a finite-amplitude instability. Solomatov and Barr (2006) estimated the absolute minimum critical Rayleigh number, Ra_{cr}^* , below which all perturbations eventually decay and the corresponding value of the aspect ratio, a_{cr}^* . Here we addressed the question: How large does a finite-amplitude perturbation have to be to initiate convection in power-law viscosity fluids? The results of our study can be summarized as follows:

1. Temperature perturbations that are most effective at driving convective motion (optimal perturbations) are located inside the rheological sublayer—in the portion of the fluid layer where the viscosity is smallest. It is possible to start convection in a fluid layer by imposing a perturbation outside of the rheological sublayer, that is in the stagnant part of the layer. Such a situation may occur in planetary mantles whose surfaces are being warmed by impacts (e.g., Reese et al., 2002). However, in this case, the onset of convection may be substantially delayed and convection will start only if a temperature anomaly of sufficiently large amplitude will be developed inside the rheological sublayer due to diffusion of the perturbation from the stagnant region into the rheological sublayer. The wavelength of the optimal perturbations is about twice the rheological sublayer thickness.
2. When the amplitude of the optimal perturbations (inside the rheological boundary layer and with the wavelength which is about twice the rheological sublayer thickness) is equal to or greater than δT_{cr}^* , Eq. (11), then the Rayleigh number required to initiate convection does not depend on the amplitude of the perturbation and is equal to Ra_{cr}^* (Eqs. (7) and (8)). For silicates at near-solidus temperatures, $\delta T_{cr}^* \approx 300$ K (e.g., for $T = 1700$ K and “wet” olivine rheology $n = 3$ and $E = 430$ kJ mol⁻¹, Karato and Wu, 1993).
3. Eqs. (25) and (26) give an estimate of the Rayleigh number necessary to initiate convection by finite-amplitude perturbations in the rheological sublayer.

Alternatively, one can estimate the critical perturbation necessary to initiate convection in a layer characterized by a particular Rayleigh number. For example, Eq. (28) suggests that if the Rayleigh number of the layer is $Ra \approx 100Ra_{cr}^*$ and the perturbation wavelength is $\lambda \approx 10\lambda_{cr}^* \approx 300$ km the amplitude of horizontal temperature variations in the rheological sublayer has to be at least $\delta T_{cr} \approx 20$ K to trigger convection.

Although we believe that this study has shed some light upon the finite-amplitude onset of convection for power-law viscosity fluids, the problem is far from being well understood and needs to be investigated in the future both numerically and theoretically.

Acknowledgments

VSS acknowledges support from NASA Planetary Geology and Geophysics Program grants NNG05GM17G and NNX06AB05G. ACB acknowledges support from NASA Outer Planets Program grant NNG05GI15G. VSS would also like to thank Boris Birger for comments and stimulating discussions.

Appendix A. Power-law viscosity without temperature dependence

Here we show that onset of convection in power-law fluids requires a substantial finite amplitude perturbation even when the viscosity does not depend on temperature. This is in stark contrast with Newtonian fluids where the finite-amplitude onset of convection below the critical Rayleigh number predicted by linear theory is only due to temperature-dependent viscosity. Also, the calculations presented below can be compared with various laboratory experiments and previous numerical calculations, thus providing an additional test for our approach. To compare our results with previous studies, we consider a square box ($a = 1$) with rigid upper and lower boundaries. The results of calculations of the critical Rayleigh number for $n = 1.1, 1.3, 2$ and 3 are shown in Fig. A.1.

Our estimates of the critical Rayleigh number are higher than the estimates obtained in previous work. This can be due to various reasons. For example, in the numerical calculations by Ozoe and Churchill (1972) whose approach is similar to ours, the Prandtl number is ~ 10 while in our calculation it is infinite. Also, Ozoe and Churchill (1972) found the critical Rayleigh number by extrapolating $Nu(Ra)$ to $Nu = 1$ rather than $Nu = Nu_{cr}^*$ (Fig. A.2). Other factors such as the difference in resolution may also play a role.

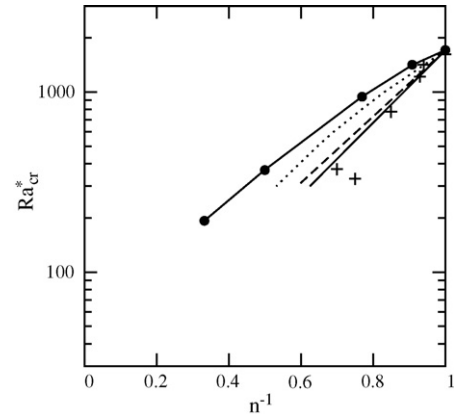


Fig. A.1. Absolute minimum critical Rayleigh number for fluids with a solely stress-dependent viscosity, as a function of the power-law exponent n^{-1} . Solid circles connected by a solid line ($n = 1.1, 1.3, 2$ and 3) are our results. Pluses correspond to the experimental data by Tien et al. (1969). The numerical results by Ozoe and Churchill (1972) are shown with a dotted line. The numerical results by Tien et al. (1969) are shown with a solid line (for two-dimensional rolls) and a dashed line (for hexagonal cells).

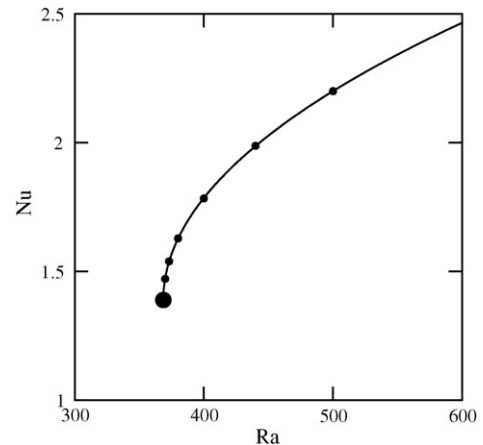


Fig. A.2. The Nusselt number as a function of the Rayleigh number near the critical point (small solid circles) for $n = 2$ and $\theta = 0$ (no temperature dependence). The parabolic fit is shown with a solid line. The critical point is shown with a large solid circle.

References

- Ansari, A., Morris, S., 1985. The effects of a strongly temperature-dependent viscosity of Stokes drag law: experiments and theory. *J. Fluid Mech.* 10, 459–476.
- Barr, A.C., Pappalardo, R.T., Zhong, S., 2004. Convective instability in ice I with non-Newtonian rheology: application to the icy Galilean satellites. *J. Geophys. Res.* 109, E12008, doi:10.1029/2004JE002296.
- Barr, A.C., Pappalardo, R.T., 2005. Onset of convection in the icy Galilean satellites: influence of rheology. *J. Geophys. Res.* 110, E12005, doi:10.1029/2004JE002371.

- Barr, A.C., McKinnon, W.B., 2007. Convection in ice I shells and mantles with self-consistent grain size. *J. Geophys. Res.* 112, E02012, doi:10.1029/2006JE002781.
- Birger, B.I., 1993. Rheology of the Earth's mantle and instability of convective flow. *Comp. Seism. Geodyn.* 3, 8–16.
- Birger, B.I., 1998. Rheology of the Earth and a thermoconvective mechanism for sedimentary basin formation. *Geophys. J.* 134, 1–12.
- Birger, B.I., 2000. Excitation of thermoconvective waves in the continental lithosphere. *Geophys. J.* 140, 24–36.
- Busse, F.H., 1967. The stability of finite amplitude cellular convection and its relation to an extremum principle. *J. Fluid Mech.* 30, 625–649.
- Chandrasekhar, S., 1961. *Hydrodynamic and Hydromagnetic Stability*. Oxford, pp. 654.
- Davaille, A., Jaupart, C., 1994. Onset of thermal-convection in fluids with temperature-dependent viscosity: application to the oceanic mantle. *J. Geophys. Res.* 99, 19853–19866.
- Dumoulin, C., Doin, M.P., Arcay, D., Fleitout, L., 2005. Onset of small-scale instabilities at the base of the lithosphere: scaling laws and role of pre-existing lithospheric structures. *Geophys. J.* 160, 344–356.
- Drazin, P.G., Reid, W.H., 1981. *Hydrodynamic Stability*. Cambridge University Press, New York.
- Drazin, P.G., 1992. *Nonlinear Systems*. Cambridge University Press, New York.
- Huang, J.S., Zhong, S.J., van Hunen, J., 2003. Controls on sublithospheric small-scale convection. *J. Geophys. Res.* 108, 2405, doi:10.1029/2003JB002456.
- Jaupart, C., Parsons, B., 1985. Convective instabilities in a variable viscosity fluid cooled from above. *Phys. Earth Planet. Int.* 39, 14–32.
- Karato, S.-I., Wu, P., 1993. Rheology of the upper mantle: a synthesis. *Science* 260, 771–778.
- Korenaga, J., Jordan, T.H., 2003. Physics of multiscale convection in Earth's mantle: onset of sublithospheric convection. *J. Geophys. Res.* 108, 2333, doi:10.1029/2002JB001760.
- Lenardic, A., Moresi, L.-N., 1999. Some thoughts on the stability of cratonic lithosphere: effects of buoyancy and viscosity. *J. Geophys. Res.* 104, 12747–12758.
- Lyubimova, T.P., 1974. O konvektivnykh dvizheniyakh nenyutonovskoi zhidkosti v zamknutoi polosti, podogrevaemoi snizu, *Izv. Acad. Nauk SSSR. Mek. Zhid. Gasa* 2, 181–184.
- Malkus, W.V., Veronis, G., 1958. Finite amplitude cellular convection. *J. Fluid. Mech.* 4, 225–260.
- McKinnon, W.B., 1999. Convective instability in Europa's floating ice shell. *Geophys. Res. Lett.* 26, 951–954.
- Moresi, L.-N., Solomatov, V.S., 1995. Numerical investigation of 2D convection with extremely large viscosity variations. *Phys. Fluids* 7, 2154–2162.
- Morris, S., 1982. The effects of strongly temperature-dependent viscosity on slow flow past a hot sphere. *J. Fluid Mech.* 124, 1–26.
- Morris, S., Canright, D., 1984. A boundary-layer analysis of Benard convection in a fluid of strongly temperature-dependent viscosity. *Phys. Earth Planet. Int.* 36, 355–373.
- Ozoe, H., Churchill, S.W., 1972. Hydrodynamic stability and natural convection in Ostwald-de Waele and Ellis fluids: the development of a numerical solution. *AIChE J.* 18, 1196–1206.
- Palm, E., 1975. Nonlinear thermal convection. *Annu. Rev. Fluid Mech.* 7, 39–61.
- Reese, C.C., Solomatov, V.S., Moresi, L.-N., 1999. Non-Newtonian stagnant lid convection and magmatic resurfacing of Venus. *Icarus* 139, 67–80.
- Reese, C.C., Solomatov, V.S., Baumgardner, J.R., 2002. Survival of impact-induced thermal anomalies in the Martian mantle. *J. Geophys. Res.* 107, 5082, doi:10.1029/2000JE001474.
- Reynolds, R.T., Cassen, P.M., 1979. On the internal structure of the major satellites of the outer planets. *Geophys. Res. Lett.* 6, 121–124.
- Richter, F.M., Nataf, H.-C., Daly, S., 1983. Heat transfer and horizontally averaged temperature of convection with large viscosity variations. *Fluid. Mech.* 129, 173–192.
- Schlüter, A., Lortz, D., Busse, F., 1965. On the stability of steady finite amplitude convection. *J. Fluid Mech.* 23, 129–144.
- Schubert, G., Turcotte, D.L., Oxburgh, E.R., 1969. Stability of planetary interiors. *Geophys. J. R. Astr. Soc.* 18, 441–460.
- Sleep, N.H., 2005. Evolution of the continental lithosphere. *Annu. Rev. Earth Planet. Sci.* 33, 369–393.
- Solomatov, V.S., 1995. Scaling of temperature- and stress-dependent viscosity convection. *Phys. Fluids* 7, 266–274.
- Solomatov, V.S., Barr, A.C., 2006. Onset of convection in fluids with strongly temperature-dependent, power-law viscosity. *Phys. Earth Planet. Int.* 155, 140–145.
- Solomatov, V.S., Moresi, L.-N., 1997. Three regimes of mantle convection with non-Newtonian viscosity and stagnant lid convection on the terrestrial planets. *Geophys. Res. Lett.* 24, 1907–1910.
- Solomatov, V.S., Moresi, L.-N., 2000. Scaling of time-dependent stagnant lid convection: application to small-scale convection on the Earth and other terrestrial planets. *J. Geophys. Res.* 105, 21795–21818.
- Solomatov, V.S., Moresi, L.-N., 2002. Small-scale convection in the D'' layer. *J. Geophys. Res.* 107, 2016, doi:10.1029/2000JB000063.
- Stengel, K.C., Oliver, D.C., Booker, J.R., 1982. Onset of convection in a variable viscosity fluid. *J. Fluid Mech.* 120, 411–431.
- Strogatz, S.H., 1994. *Nonlinear Dynamics and Chaos*. Westview Press, Cambridge, MA.
- Tien, C., Tsuei, H.S., Sun, Z.S., 1969. Thermal instability of a horizontal layer of non-Newtonian fluid heated from below. *Int. J. Heat Mass Transf.* 12, 1173–1178.
- Yuen, D.A., Peltier, W.R., 1980. Mantle plumes and the thermal stability of the D'' layer. *Geophys. Res. Lett.* 7, 625–628.
- White, D.B., 1988. The planforms and onset of convection with a temperature-dependent viscosity. *J. Fluid. Mech.* 191, 247–286.